ISET Journal of Earthquake Technology, Paper No. 576, Vol. 60, No. 1, March 2023, pp. 1–25

PERFORMANCE BASED SEISMIC EVALUATION BEYOND IMMEDIATE OCCUPANCY LEVEL OF EXISTING RC STRUCTURES USING CONTROL AND STRENGTHENING TECHNIQUES

Milan Nakum (Corresponding Author)
Post Graduate Student, Department of Structural Engineering
Veermata Jijabai Technological Institute (VJTI), Matunga, Mumbai
E mail id: *nakummilan11@gmail.com*

G Rami Reddy
Adjunct Professors, Department of Structural Engineering
Veermata Jijabai Technological Institute (VJTI), Matunga, Mumbai
E mail id: *grrddy@yahoo.com*

ABSTRACT

Structures are commonly subjected to normal loads as well as accidental loads caused by earthquakes. According to the standards, structures are designed employing a force-based method. The provisions in the code are meant to prevent collapse during earthquakes, and the performance of a structure is evaluated qualitatively. This Paper aims to understand that the performance of existing structures against seismic loads can be improved by adopting the Performance Based Seismic Design (PBSD) approach. Performance based design helps in achieving the targeted performance level of a structure like Operational (O), Immediate Occupancy (IO), Life Safety (LS) and Collapse Prevention (CP). The use of Strengthening methods or Response control methods of retrofitting can provide better performance for existing structures subjected to earthquakes. Earlier researchers have performed retrofitting using a combination of Friction damper and steel bracing of Reinforced Concrete (RC) buildings and achieved the IO performance level. If performance levels are beyond IO, structural elements and components will see nonlinear deformations causing energy dissipation. If control methods and strengthening methods are used to improve the performance of the existing RC structure, the effect of energy dissipation in the elements and components needs to be considered while evaluating the responses. This aspect was not considered earlier and proposed to be investigated in the present work. The 5-story RC building is considered and is retrofitted with a Friction damper and steel bracings in the present work to achieve the desired performance beyond the IO level. Pushover analysis is performed with the help of SAP2000 (2021) to determine the structure's realistic capacity and element energy dissipation based on the user-defined hinge characteristics and the Time history analysis is performed to get the energy dissipation from dampers. The methodology of retrofitting to reach the desired performance level is provided and a comparison of results before and after retrofitting of the structure is made.

KEYWORDS: Capacity, Demand; Earthquake; Hinge; Performance Based Seismic Design; Performance Level; Retrofitting; Seismic Evaluation

INTRODUCTION

In the past, there had been several destructive earthquakes (NICEE, 2023; USGS, 2023) and RC structures suffered significant damage, along with numerous fatalities and financial losses. Design professionals select the proportions and details of building components to meet prescriptive requirements as stated in regional codes (IS:456, 2000; IS:1893 (Part-1), 2016) in a conventional structural design process (i.e., forces-based design). The code describes required minimum levels of strength, stiffness modifiers, identifies acceptable structural and non-structural safety, specifies material properties and construction details and methods of how a structure is to be designed and built. Seismic design codes presently rely on a force-based approach, wherein calculations determine forces and displacements within elastic limits for designing structural and nonstructural components. These calculations are then utilized in the design process. Displacement limits, drift limits and crack widths are used to meet serviceability requirements.

The response reduction factor as shown in Figure 1, which relates to ductility, over-strength, and redundancy is used to reduce the response forces evaluated in the elastic method. This factor is also used to

evaluate nonlinear deflection to check the serviceability limit. However, such an indirect approach leads to misjudgment of the actual building response. Additionally, these processes are indirect and unreliable, resulting in expensive and inefficient structures. Strong earthquakes induce nonlinear behaviors in reinforced concrete structures. Current code-based design philosophies do not explicitly include the inelastic response of structures in their considerations (Zameeruddin and Sangle, 2021). At the same time, the PBSD enables estimating the required performance of structures for the given design basis loading. Acceptance criteria in terms of plastic rotation angle for Beam, Column, and Beam-Colum Joints are provided along with the permissible drifts of the structures (Armaly et al., 2019; Chaudhury and Singh, 2014).

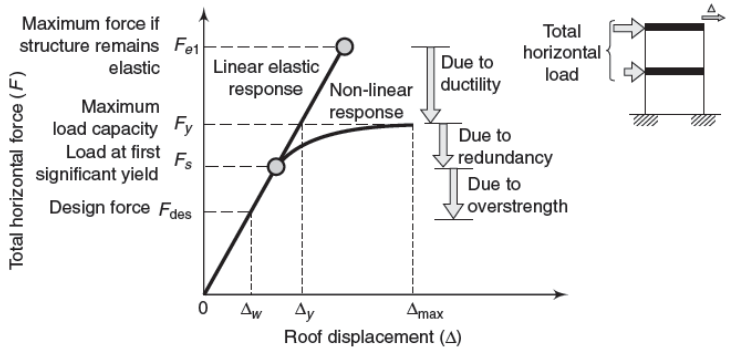

Fig. 1 Response Reduction Factor (Patel and Shah, 2010)

The PBSD enables structures to be designed with a realistic and reliable understanding. PBSD defines different target Building Performance Levels as shown in Figure 2.

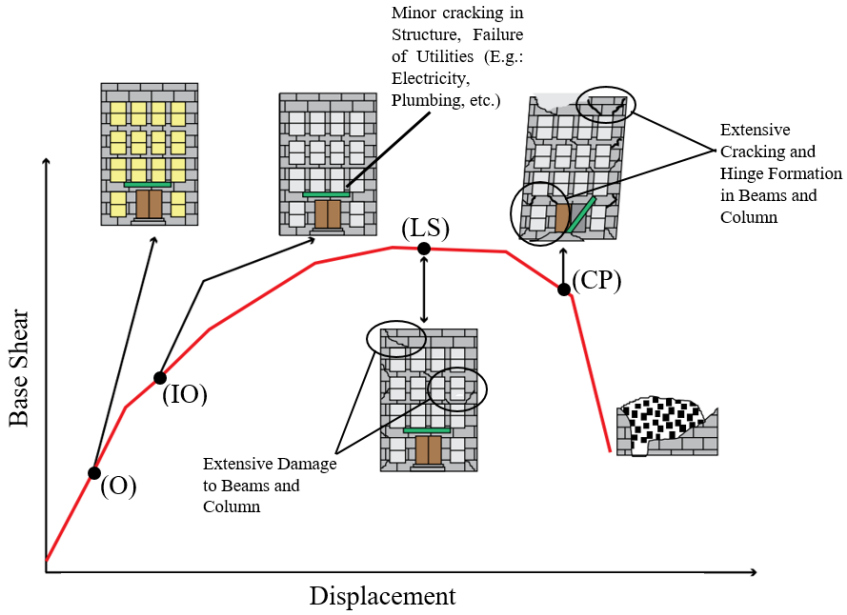

Fig. 2 Seismic Performance Levels of Structure (Golesorkhi et al., 2019)

The Operational (O) Performance Level is expected to sustain minimal or no damage to its structural and nonstructural components. Immediate Occupancy (IO) Performance Level is expected to sustain minimal or no damage to their structural elements and only minor damage to their nonstructural components. Life Safety (LS) Performance Level may experience extensive damage to structural and nonstructural components. Collapse Prevention (CP) Performance Level may experience extensive damage to structural and nonstructural components (ASCE 41, 2013; FEMA 356, 2000).

LITERATURE REVIEW

In the literature, research studies are seen on seismic evaluation and seismic retrofitting to enhance the performance of structures using strengthening and response control techniques. The presented research work on retrofitting shows improved response of the structure and IO performance level is achieved, where

analysis is done based on default hinges (Chaudhury and Singh, 2014; Gupta et al., 2022). Gupta et al. (2022) studied five-story reinforced concrete (RC) buildings retrofitted with friction dampers and steel bracing to achieve a target seismic performance level in terms of inter-story drift and plastic hinge rotations. The peak roof displacement of a building with damper plus bracing reduces by 80.42 %, and 80.58 % in the X and Y directions respectively. The combination of friction damper and steel bracing was found to be effective in retrofitting five-story RC buildings with all the plastic hinge rotation in members within the IO performance level. Chaudhury and Singh (2014) developed a step-by-step design procedure for a structure with yielding and friction damper. This methodology was used to achieve the target performance level (IO) in terms of inter-story drift and plastic hinge rotation. Results show that friction and metallic dampers are helpful in reducing roof displacement and building inter-story drift. It was discovered that both of the dissipation systems significantly enhanced the building's performance. Moon et al. (2017) proposed a method for the design of friction damping systems for the seismic retrofit of low- to mid-rise regular reinforced concrete (RC) buildings. The building was retrofitted using a friction damping system consisting of braces and friction dampers. The friction damper was observed to dissipate as much as 62% of the total energy dissipated by the retrofitted structure. Badoux and Jirsa (1990) examined the use of steel bracing systems for retrofitting seismically inadequate reinforced concrete frames. A reinforced-concrete frame was retrofitted with steel bracings. The bracing scheme significantly improved the strength, stiffness, and ductility of the frame. A brace with very low slenderness yields instead of buckling in compression, ensuring significant hysteretic energy dissipation through yielding and inelastic buckling of the braces. Steel bracings are versatile and can be used to achieve a variety of objectives, ranging from drift control (serviceability state) to collapse prevention (ultimate state). The studies suggest the use of Damper and Steel bracings are beneficial in improving the performance of an existing RC structures.

1. Friction Dampers in Retrofitting of Structures

Friction dampers absorb energy through the friction between rubbing surfaces, akin to the mechanism of brakes used to halt the motion of various vehicles and equipment. When the friction force at the interface exceeds the limiting frictional force, the friction damper initiates energy dissipation. This type of damper provides damping irrespective of loading velocity and ambient temperature and is typically installed parallel to bracing sections (Jia, 2017). The force-displacement loop for friction dampers, illustrated in Figure 3, exhibits substantial rectangular hysteresis loops with minimal fading, resembling ideal elasto-plastic behavior and offering effective energy dissipation. Additionally, friction dampers feature a relatively high starting stiffness and nearly rectangular angular hysteretic behavior, maintaining near-constant peak force as displacement changes. Comparatively, for a given maximum force, the hysteresis loop area (energy dissipation or damping) of a viscous damper is approximately 70% that of a friction damper. This implies that 70 friction dampers achieve the same damping as 100 viscous dampers. Conversely, for a given number and damping amount, friction dampers exert only 70% of the forces exerted by viscous dampers. This saves money on dampers, bracing, connections, columns, and foundations (Pall and Pall, 2004).

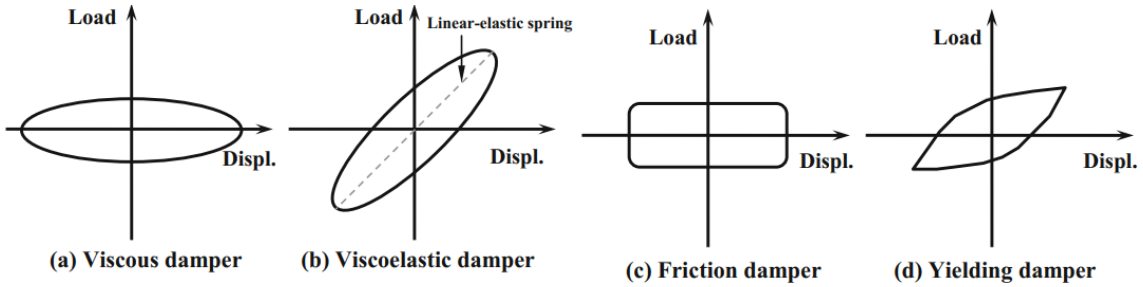

Fig. 3 Force-displacement curve for different types of dampers (Jia, 2017)

The most common type of friction damper is the pall friction damper. Pall and Marsh (1982), developed it based on the automotive brake, and it can be incorporated as part of bracing or as joints. In Figure 4, hinged links are arranged to form a quadrilateral shape, with two diagonal links hinged at the joints of the horizontal diagonal bracing. Each diagonal link within the quadrilateral region consists of two separate components partially superimposed by a friction brake joint positioned in the damper's center. Both braces are active and respond elastically in tension and compression before the friction damper slips. When the seismic load is applied, the damper slips at a predefined optimum load before the primary structure yields, leading to compression braces buckling and experiencing considerable deflections, while tension braces remain elastic within certain seismic load levels. As the seismic load increases, the exterior buckled braces

remain subject to the same critical buckling load. However, the tension brace begins to produce slippage at the friction joint, and the relevant friction force is determined by setting the clamp force and friction coefficient of the dampers. This activation of the four links causes the compression brace to slip. When the load is reversed, the brace initially under compression can absorb tension energy. Following a loading cycle, the resulting loop areas for both braces are identical (Jia, 2017).

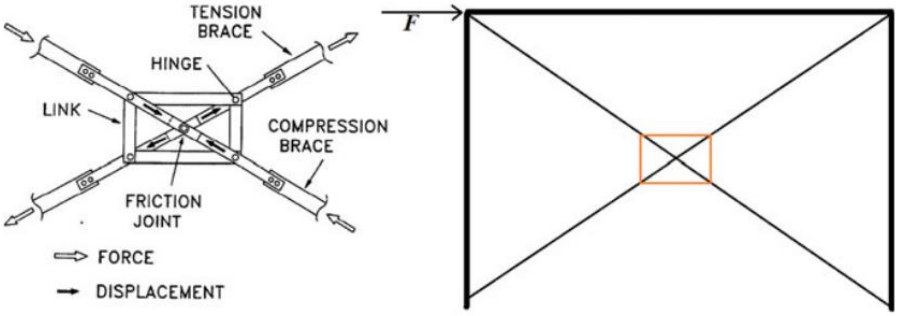

Fig. 4 Pall friction damper and its location in braced system (Jia, 2017)

The benefits of incorporating friction dampers encompass higher energy dissipation for a given force, as illustrated in Figure 3. They are straightforward to install, compact, and narrow enough to fit inside partitions. Performance remains unaffected by loading velocity or temperature. As passive energy dissipation devices, friction dampers operate without the need for an external energy source and become active during earthquakes. Their cost-effectiveness is reflected in low maintenance expenses, given the absence of components prone to deterioration and leakage. This eliminates the necessity for routine inspection, maintenance, repair, or replacement before (and potentially after) earthquakes. While acknowledging potential wear on the friction surface, it's noteworthy that the maximum force on a friction damper is constant and well-known, facilitating the uncomplicated and economical design of these members.

Couch et al. (2023) have investigated the structural characteristics of an ordinary-low ductility moment frame and concentrically braced frame with a friction damper. The inline friction damper manufactured by Quaketek having a slip load of 22 kN was used in the test. The friction-damped braced configuration reduced the frame acceleration on average by 25.26 per cent. Armaly et al. (2019) investigated the effectiveness of implementing friction dampers as a passive dissipative device and proposed a certain optimization of the quantity and location of dampers in the building. According to the analysis's findings, the structure's natural time period has been changed to a lower value as a result of the addition of friction dampers. In terms of time, the reduction equal to 21.5% of the 1st Mode is observed. Compared to the conventional shear wall system of the same building, the reaction of the structure provides a reduction in roof floor acceleration of 31.22%, roof displacement of 50%, base shear of 43.77%, and storey drift of 58.53%. In their study, Sadeghi et al. (2021) examined the impact of friction dampers on response modification factors (R), including ductility and over-strength. They utilized an idealized bilinear response capacity curve in steel structures, considering both traditional and advanced nonlinear static analysis (multi-modal) methods. The findings indicate that as the number of dampers increases, the structure's response modification factor rises, implying a decreased earthquake demand for structures equipped with friction dampers.

To obtain the realistic capacity of the structure, the user defined hinge characteristics are considered. Under both monotonic and cyclic loading patterns, several reinforced concrete beam-column joints were tested and simple and clear numerical procedures to calculate the load-deformation characteristics are proposed using (Kent and Park, 1971) constitutive relationship (Sharma et al., 2009). The joint DB312M is considered for validating the procedures explained further. Compressive strength of 19.6 MPa, Fe500 reinforcements (IS:456, 2000), and the effect of buckling for reinforcements in the compression zone are considered (Dhakal and Maekawa, 2002) for evaluation of Moment-Rotation. The details of T shaped Beam-Column joint, and the comparison of the Moment-Rotation curve from experimental and numerical results obtained using specified procedure are shown in Figure 5 (a, b) respectively. The capacity of the joint is observed closely matching the author's results in user-defined hinge cases, while higher capacity is obtained based on the default hinge analysis based on Mander et al. (1988) model Default in SAP2000 (2021). Hence, the User-defined Hinge procedures are adopted to obtain the capacity of G+4 Storey RC structure. The results of User-defined hinges and Default hinges based will be compared.

PROCEDURE FOR PERFORMANCE EVALUATION OF EXISTING STRUCTURES

Demand and capacity are the two primary objectives of a performance-based seismic evaluation technique. The ground motion of an earthquake is represented by demand. The ability of a structure to withstand seismic demand is represented by its capacity. The various steps involved in evaluating performance levels for given seismic demand are as follows:

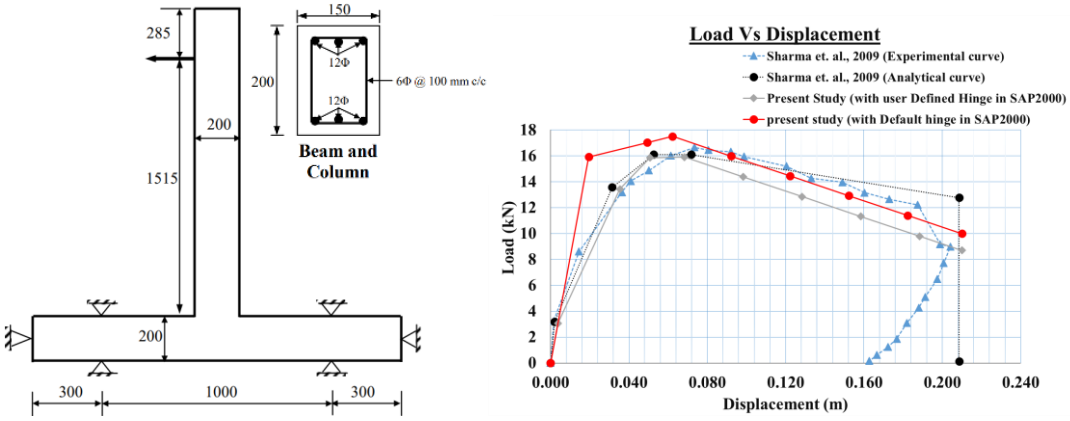

Fig. 5 (a) Joint Details, Beam and Column Details (b) Capacity of joint

In the first step, capacity of the structure is generally obtained using nonlinear static analysis (Push over analysis) in terms of base shear v/s roof displacement. It is converted into capacity spectrum in terms of acceleration v/s displacement using the procedure explained in ATC 40 (1996). In the second step selected design spectrum given in the codes is converted into Acceleration Displacement Response Spectrum (ADRS) as explained in ATC 40 (1996). In the third step these two spectra are superposed and evaluated the intersection point. This intersection point gives initial performance level in terms acceleration vs. roof displacement. In the fourth step new damping is evaluated considering the hysteresis, limiting the displacement as evaluated above and corresponding force in the capacity of the structure. With the new damping, demand spectrum is modified and new intersection point is evaluated and thirst and fourth steps are repeated till convergence in performance point is achieved. The graphical representation of the evaluation procedure is shown in Figure 6 (a-d). If the required performance level is not met, retrofitting the structure is recommended. The detailed procedures are explained in a further part for evaluating the capacity of the structure.

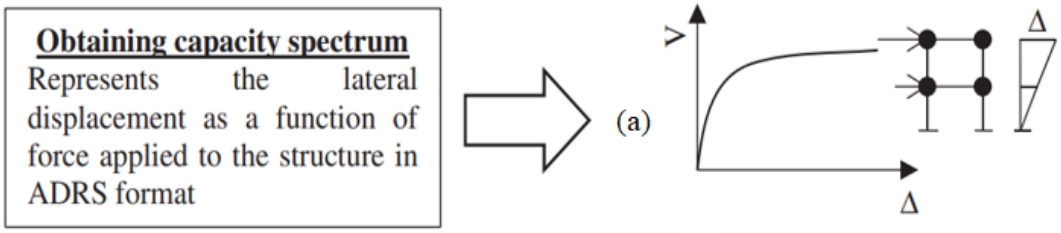

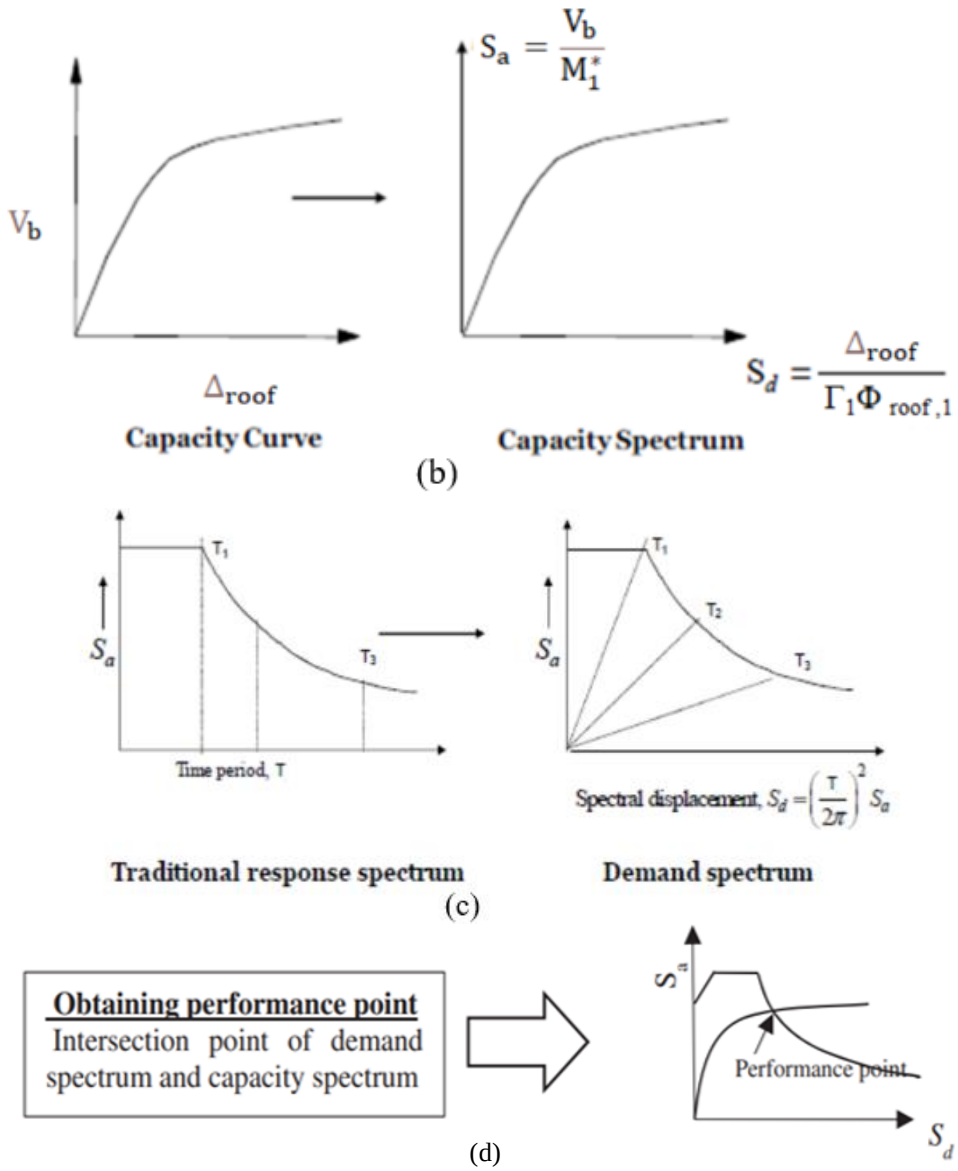

Fig. 6 (a-d) Performance Evaluation by Capacity spectrum method (Zameeruddin and Sangle, 2021; Gupta, 2021)

1. Details of Existing RC Structure

The details of structure is taken from the work of Gupta et al. (2022). SAP2000 (2021) is used to model a G+4 Storey RC building with floor-to-floor heights of 3 m, 5 bays of 4 m span, and 3 bays of 5 m span in the X and Y directions, respectively as shown in Figure 7. Both the steel and concrete utilized are of the M 25 and Fe 415 grades, respectively. As indicated in Figure 8, 230 x 500 mm beams, 300 x 300 mm columns, and a slab 120 mm thick are employed. The model is applied with a live load of 3 kN/m^2 on all floor levels, a floor finish of 1.5 kN/m^2, a roof finish of 2 kN/m^2, external wall loads of 9 kN/m, and parapet wall loads of 3 kN/m on the roof floor. According to the building's modal analysis, the fundamental period is 1.0688 sec in the Y direction and 1.0199 sec in the X direction.

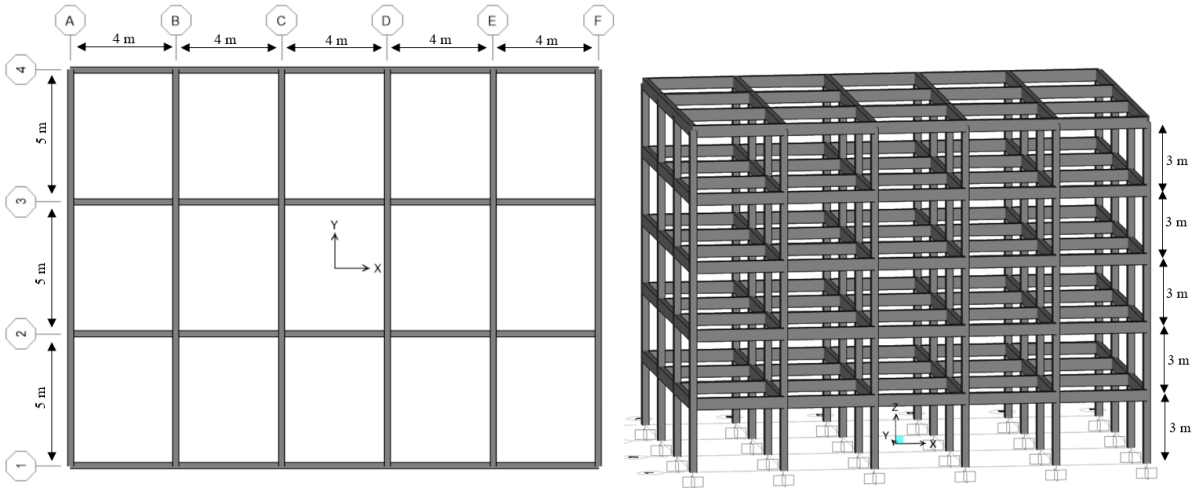

Fig. 7 (a) Plan (b) 3D Views of G+4 Storey RC Structure

2 Non-Linear Static Procedures (Pushover Analysis)

Load deformation characteristics i.e. moment-curvature or moment-rotation of the hinge portion of the beam, column and joint are the basic requirement to start with Pushover analysis. The details of the beam, column shown in Figure 8 are used to generate material properties and element moment-rotation characteristics. The procedure is divided into two major steps i.e. Material properties and Element load deformation characteristics.

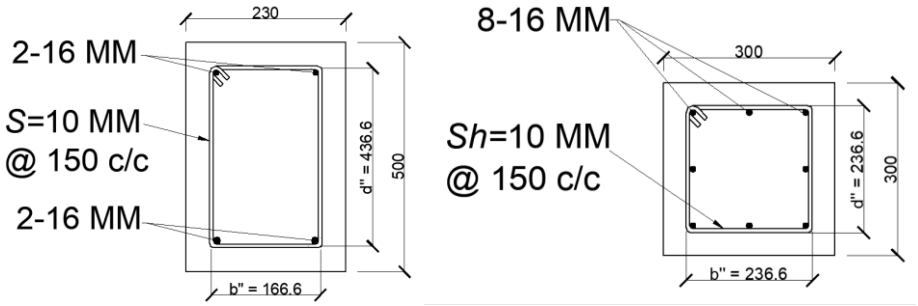

Fig. 8 (a) Beam (b) Column

Material Properties: The material properties include the Confined concrete model and reinforcement steel model. Since design is done as per (IS:456, 2000) for the confining effect of concrete, the Kent and Park (1971) model without an increase in strength is selected, with Fe415 reinforcement steel based on IS:456 (2000) which is also modified to account for the buckling effect.

Confined Concrete (Kent and Park, 1971) Model: As non-ductile detailing is utilized following (IS:456, 2000), Figure 9 depicts material property for concrete confined with rectangular stirrups. The highest stress attained by confined concrete is equal to the cylinder strength f_c' at 0.002 strain (Sharma et al., 2009).

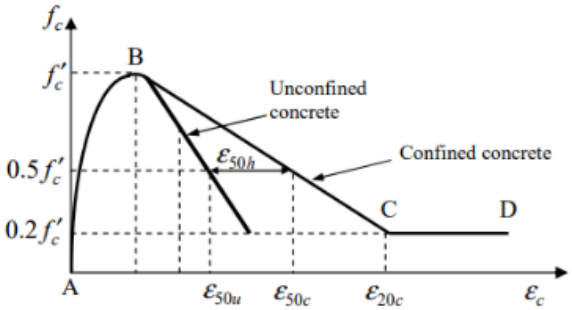

Fig. 9 Confined Concrete model (Sharma et al., 2009)

The ascent parabolic relation of the curve is expressed as, Region AB, $\varepsilon_c \leq 0.002$

$$f_C = f_C^{'}\left[1 - Z(\varepsilon_C - 0.002)\right] \tag{1}$$

The post-peak part of the curve is given as follows.

Region BC, $0.002 \le \varepsilon_C \le \varepsilon_{20c}$

$$f_C = f_C^{'}\left[1 - Z(\varepsilon_C - 0.002)\right] \tag{2}$$

where,

$$Z = \frac{0.5}{\varepsilon_{50u} - \varepsilon_{50h} - 0.002};\ \varepsilon_{50u} = \frac{3 + 0.002 f_C^{'}}{f_C^{'} - 1000};\ \varepsilon_{50h} = \frac{3}{4}\rho_s\sqrt{\frac{b''}{s_h}} \tag{3}$$

$f_C^{'}$ = Cylinder strength of concrete in psi, ρ_s = Ratio of the vol. of transverse reinforcements to the vol. of concrete core measured to the outside of stirrups

$$\rho_S = \frac{2(b'' + d'')A_S}{b''d''s_h} \tag{4}$$

A_s = c/s area of the stirrup, s_h = Spacing of stirrup

b'' and d'' = Width and Depth of confined core measured to the outside of stirrup

Region CD, $\varepsilon_C \ge \varepsilon_{20c}$

$$f_C = 0.2 f_C^{'} \tag{5}$$

The capacity of concrete to withstand 20% stresses at very large strains is taken into account by this equation. Putting, $f_C = 0.2 f_C^{'}$ and $\varepsilon_C = \varepsilon_{20c}$ in equation (2), we get

$$\varepsilon_{20c} = \frac{0.8}{Z} + 0.002 \tag{6}$$

The material properties of Beam and Column are obtained as shown in Figure 10.

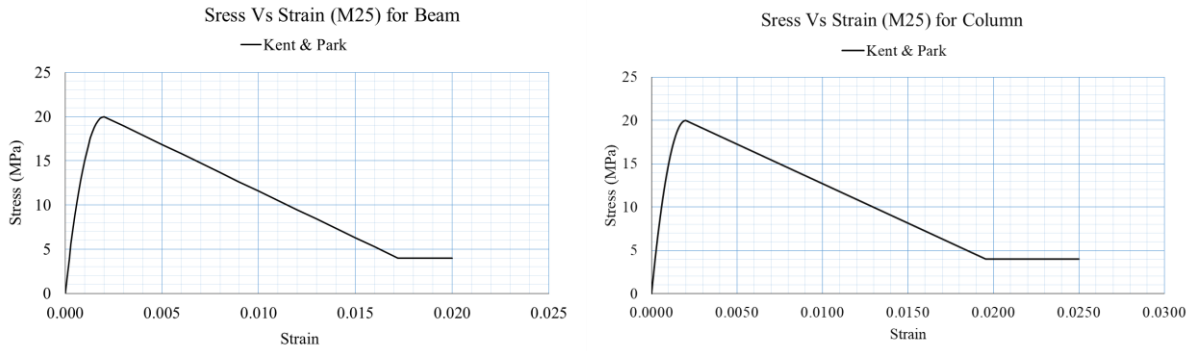

Fig. 10 Stress-Strain Model of Confined Concrete (a) Beam (b) Column

Reinforcement Steel Model (Fe415 including Buckling): E_s is taken as 200000 N/mm^2. The Reinforcement Steel model considered is elastic-perfectly plastic as per (IS:456, 2000). The stress-strain relationship for steel in tension and compression is assumed to be the same. However, the steel starts buckling in the compression zone when the concrete starts crushing at the plastic hinge formation. The reinforcement steel model with the buckling effect is shown in Figure 11. The following steps are followed for obtaining a monotonic compressive stress-strain relationship of reinforcement steel,

$$\sigma_{sc} = E_S\,\varepsilon_{sc} \text{ for } \varepsilon_{sc} \le \varepsilon_y \tag{7}$$

$$\frac{\sigma_{sc}}{\sigma_t} = 1 - \left(1 - \frac{f_i}{f_{it}}\right)\left(\frac{\varepsilon_{sc} - \varepsilon_y}{\varepsilon_i - \varepsilon_y}\right) \text{ for } \varepsilon_y \le \varepsilon_{sc} \le \varepsilon_i \tag{8}$$

$$\sigma_{sc} = f_i - 0.02E_S\left(\varepsilon_{sc} - \varepsilon_i\right);\ \sigma_{sc} \ge 0.2 f_y \text{ for } \varepsilon_{sc} \ge \varepsilon_i \tag{9}$$

$$\frac{\varepsilon_i}{\varepsilon_y} = 55 - 2.3\sqrt{\frac{f_y}{100}}\frac{L}{D};\ \frac{\varepsilon_i}{\varepsilon_y} \ge 7 \tag{10}$$

$$\frac{f_i}{f_{it}} = \alpha\left(1.1 - 0.016\sqrt{\frac{f_y}{100}}\frac{L}{D}\right);\ \frac{f_i}{f_{it}} \ge 0.2 \tag{11}$$

where, σ_t = Stress in the tension for ε_{sc} (compression strain),

σ_{sc} = Compressive Stress, f_{it} = Stress in the tension curve corresponding to ε_i ,

f_i = Stress in the Compression curve corresponding to ε_i , ε_i = Strain at the intermediate point, L = Plastic hinge Length of the corresponding section, D = Diameter of the longitudinal Reinforcing bar, α = 0.75 for Elastic Perfectly plastic bars.

Element Load Deformation Characteristics: Load deformation of element (Beam and Column) depends on Hinge. The strength and deformation in terms of moment and corresponding rotation that the member will experience are depicted on a plot called the moment rotation for an element, which is generated from the moment-curvature properties of its section. The section analysis of the beam/column is shown in Figure 12.

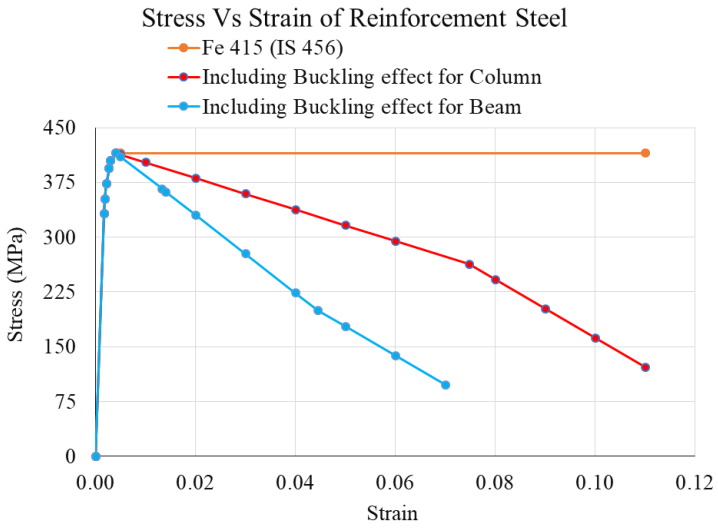

Fig. 11 Stress-Strain Model of Reinforcement

Moment Curvature: The procedure to obtain the moment-curvature is as follows,

i) Assume a strain value at the outermost compression fiber of concrete, ε_{cm}.

ii) Assume a neutral axis depth value, *kd*.

iii) Obtain stress block parameters α and γ for the selected value of ε_{cm} (Sharma et al., 2009).

iv) Obtain, C_{con} (Compressive force of concrete) using eq. (14).

v) Using eq. (12), calculate the strains and the corresponding stresses in reinforcing bars based on the material property of steel.

vi) Obtain the compression (C_{si}) and tension (T_{si}) forces in the reinforcing bar by eq. (13) and see whether the force equilibrium condition eq. (15) is fulfilled.

vii) If eq. (15) is fulfilled, which means the *kd* is correct. Else take a fresh value of *kd* and proceed to step *(iv)*.

viii) Calculate the moment, M using eq. (16), and curvature, φ using eq. (17).

ix) Repeat steps *(i)* to *(ix)* for a value of ε_{cm} and plot the M- φ curve.

x) Calculate the Rotation corresponding to the Curvature using eq. (18-19).

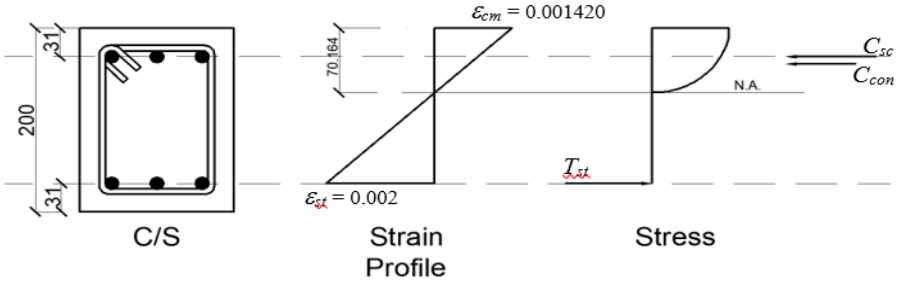

Fig. 12 Theoretical moment-curvature determination (Sharma et al., 2009)

$$\varepsilon_{si}=\varepsilon_{cm}\frac{kd-d_i}{kd} \tag{12}$$

$$C_{si} \text{ or } T_{si} = f_{si} A_{si} \tag{13}$$

$$C_{con} = \alpha f_c^{'} bkd \tag{14}$$

$$P=\alpha f_c^{'} bkd+\sum_{i=1}^{n} f_{si}A_{si} \tag{15}$$

$$M=\alpha f_c^{'} bkd\left(\frac{D}{2}-\gamma kd\right)+\sum_{i=1}^{n} f_{si}A_{si}\left(\frac{D}{2}-d_i\right) \tag{16}$$

$$\varphi=\frac{\varepsilon_{cm}}{kd} \tag{17}$$

where,

n = Nos. of reinforcing bars, f_{si} = Stresses in the i^{th} bars, A_{si} = Areas of i^{th} bars

D = Overall depth of the member, d = Effective depth of the member, d_i = depth of bar i^{th} from extreme compression fiber.

Equivalent Compressive Stress Block Parameters (α, γ): For various values of ε_{cm} depending on if ε_{cm} falls in region AB, BC, or CD of the concrete model the parameters are calculated using the equations provided in the work of Sharma et al. (2009).

Determination of Moment-Rotation: The definition of curvature is a rotation of a member per unit length. Once we have the curvature values the rotations can be calculated using the following formulas.

$$\theta_y = \frac{\varphi_y l_p}{2} \text{ and } \theta_P = \left(\varphi_u-\varphi_y\right) l_p \tag{18}$$

$$\theta_u = \theta_y + \theta_P \tag{19}$$

where, l_p = 0.5d, l_p = Plastic hinge length, φ_u = Ultimate Curvature, φ_y = Yield Curvature, θ_u = Ultimate Rotation, θ_y = Yield Rotation, θ_p = Plastic Rotation, d = Effective depth of the member

3. Non-Linear Analysis Procedures

The calculated Moment Rotation Characteristics are then normalized with the yield moment and yield rotation of the section to provide it as the input in SAP2000 (2021) and it was defined as M3 hinges (flexure hinge) for the Beam and Column section as shown in Figure 13. After that the displacement-controlled non-linear load cases are defined to perform the Pushover Analysis. The nonlinear load cases namely Gravity-NL and Push-x, Push-y with lateral load pattern are defined concerning the fundamental mode in the X and Y directions respectively.

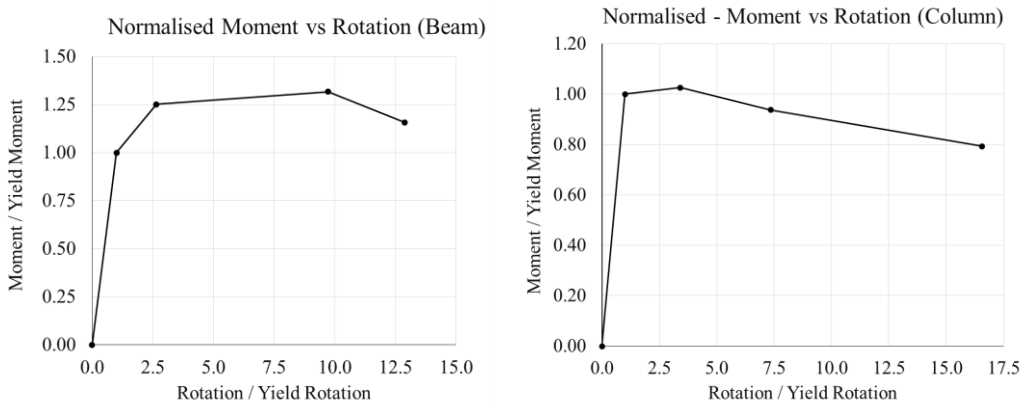

Fig. 13 Moment Rotation Characteristics of Beam and Column for User defining Hinge

After assigning the hinges analysis was performed and the Capacity curve was obtained. The capacity curve obtained using User-defined hinges and Default Hinges available in SAP2000 (2021) is compared as

shown in Figure 14. There is a significant difference observed in the capacity of the structure obtained. The capacity of the structure is overestimated in Default hinge cases which was observed same in Beam-column joint validation.

4. Performance Level Acceptance Criteria

The parameters and Criteria provided in ASCE 41 (2013), clause 10.4 are used as the acceptance criteria for the rotations of the Beam and Column. The criteria mainly depends on the Confinement and Non confinement of the sections, Reinforcement ratios and design shear force as mentioned in the code. The Figure 15 shows generalized acceptance criteria, where P stands for Primary elements and S sands for secondary elements. Following the procedures of ASCE 41 (2013), the acceptance criteria are calculated for Beam and Column as shown in Table 1. The criteria shown in Table 1 are marked on the calculated moment rotation characteristics of the elements (in Section 3.3) are shown in Figure 16 (a) and (b) for Beam and column respectively.

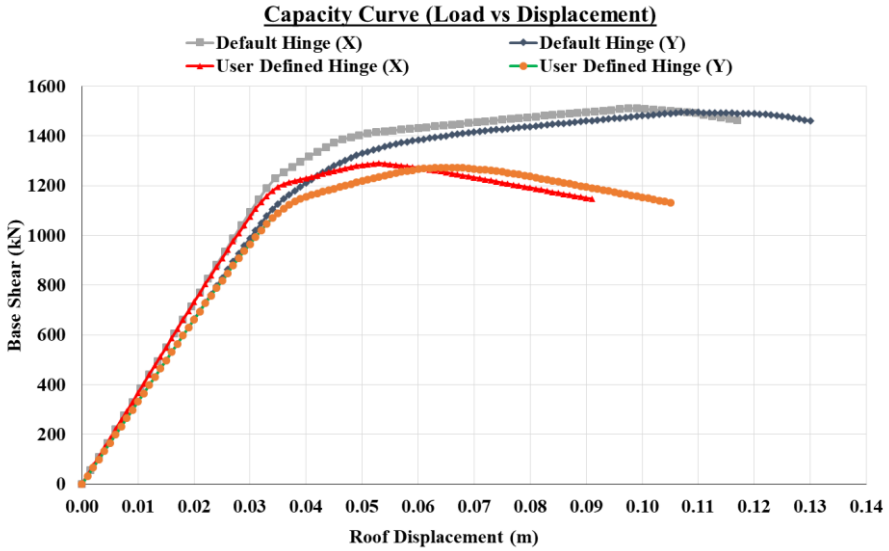

Fig. 14 Capacity curves Comparison

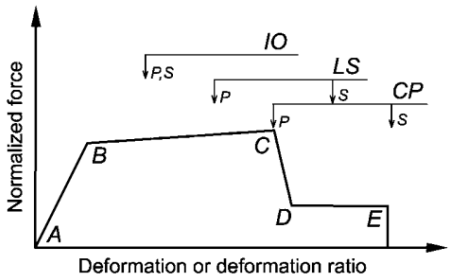

Fig. 15 Acceptance Criteria Illustration (ASCE 41, 2013)

Table 1: Performance criteria based on Rotations (ASCE 41, 2013)

Performance Level	Beam	Column
	Rotation (rad)	Rotation (rad)
IO	4.89	1.72
LS	7.29	2.56
CP	9.73	3.42

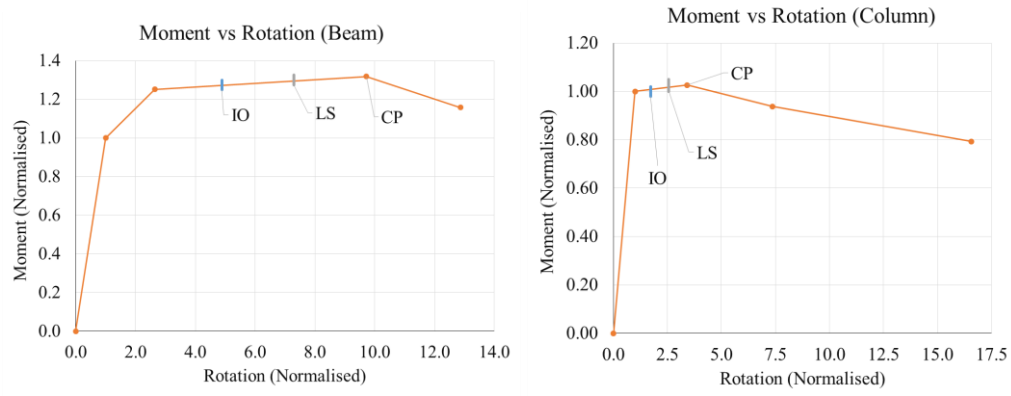

Fig. 16 Rotation based Acceptance criteria for (a) Beam (b) Column

Once the Pushover analysis is completed, the step by step Moment-rotation data can be obtained for each elements of the structure. The performance level based on the rotations of the elements is marked on the capacity curve of structure for user defined hinge case as shown in Figure 17. After defining the performance criteria, the capacity-demand spectrum of structure is prepared. Here, the Design Basis Earthquake (DBE) level demand spectrums from IS:1893 (2016) are considered for all zones with Soil Type II. The capacity-demand spectrum of structure along with performance levels and demand spectrum of IS:1893 (2016) is shown in Figure 18.

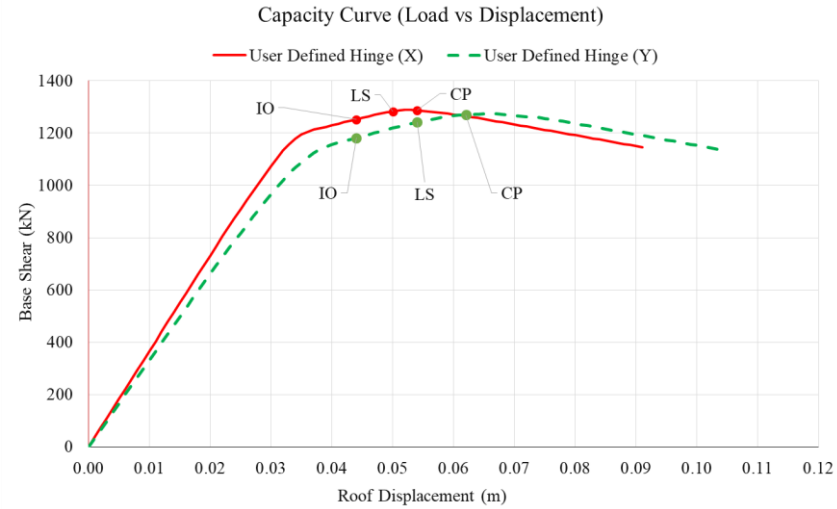

Fig. 17 Capacity curve with Rotations based Performance levels

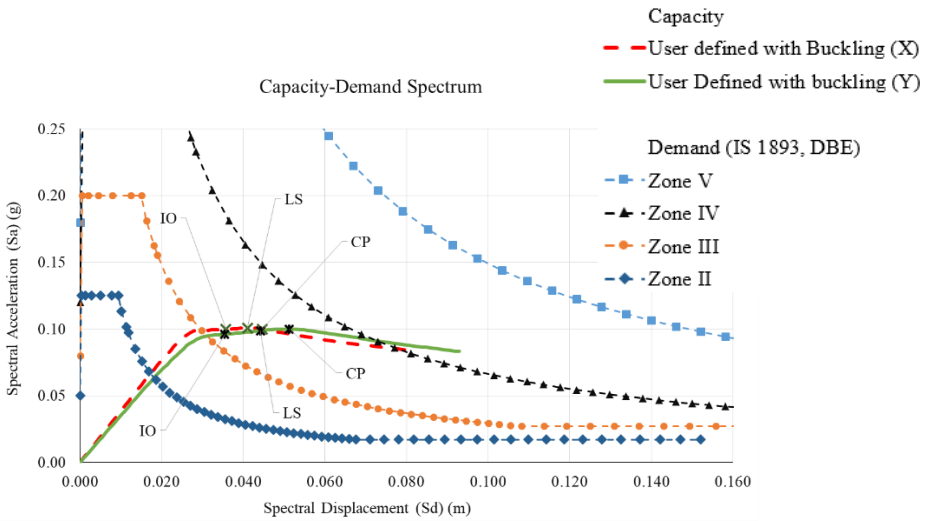

Fig. 18 Capacity-Demand Spectrum of Structure

From the Figure 18 it can be seen that the capacity curve of structure is not meeting the demand spectrum of Zone V as the demand is quite huge. The Capacity is intersecting with Zone IV demand curve but it is in collapse prevention level. Further the Zone III demand is intersecting within IO level and the Zone II demand is observed in Operational level itself. It is quite surprising to observe that the structure design for the gravity loads only is qualifying the performance level beyond IO level. It is to be noted that, since the joints are assumed as a rigid in analysis, this behavior is considered and to maintain the rigidity of joints in structure the local strengthening is necessary for rigid behavior (i.e., Haunch, FRP laminates, etc.). Further the demand of Zone IV is considered in the present study and the structure will be qualified for the desired performance level of the same.

5. Element Energy Dissipation

The area under the moment rotation curve is considered as Energy dissipated through the element. Once the hinge is yielded, the area under moment Rotation curve is calculated and the Energy dissipated by formation of hinge is obtained. Damping during earthquake ground motion pushing a structure into the inelastic range results from the combination of inherent viscous damping and hysteretic damping. Hysteretic damping is associated with the area inside the loop formed when plotting Moment against the Rotations of the structure. Equations from the literature (ATC 40, 1996) allow representing hysteretic damping as equivalent viscous damping. The equivalent viscous damping, β_{eq}, associated with a Plastic Rotation of θ_p, can be estimated from the following equation,

$$\beta_{eq} = \beta_0 + 0.05 \tag{20}$$

where,

β_0 = hysteretic damping represented as equivalent viscous damping

0.05 = 5% viscous damping inherent in the structure

The term β_0 can be calculated as:

$$\beta_0 = \frac{1}{4\pi}\frac{E_D}{E_{so}} \tag{21}$$

where, E_D = Energy dissipated by Element, E_{so} = Strain energy of the structure

E_D is the energy dissipated by the Element in a single, that is, the area enclosed by a single hysteresis loop.

Strain energy (E_{so}) = Force × Displacement = $F_i \times \delta_i$

where, F_i = Forces at i^{th} node and δ_i= deflection at i^{th} node.

$$E_{so} = \sum \frac{1}{2} \times F_i \times \delta_i \tag{22}$$

Following the above procedures, the total Energy dissipated by Element from total numbers of yielded hinges during Pushover analysis is calculated. The total energy dissipated in X and Y direction is shown in Table 2.

Table 2: Element Energy Dissipation from Hinges

Description	X direction	Y direction
Total Energy Dissipation ***(E_D)*** (kN-m) =	88.126	64.458
Strain Energy ***(Eso)*** (kN-m) =	255.038	220.255
Hysteresis damping ***(β_o)*** =	0.027	0.023
Inherent damping ***($\beta_{elastic}$)*** =	0.050	0.050
Equivalent Damping ***(β_{eq})*** =	0.077	0.073

Now, after accounting the Element energy dissipation of the structures the reduced demand spectrum of 7.7% and 7.3% damping is generated from the 5% damped (IS:1893, 2016) Zone IV response spectrum. The Figure 19 and Figure 20 shows the Capacity-Demand Spectrum with reduced Damping demand spectrum.

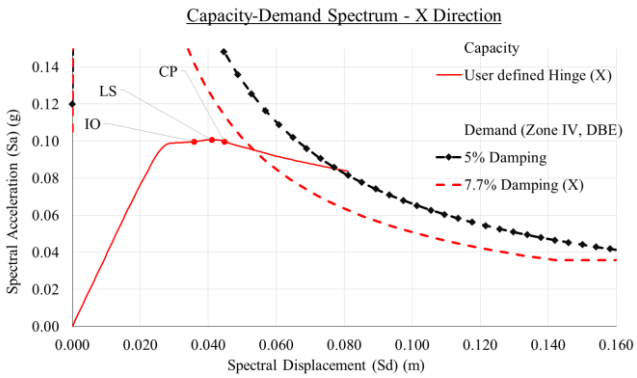

Fig. 19 Capacity-Demand Spectrum with Damping (X – Direction)

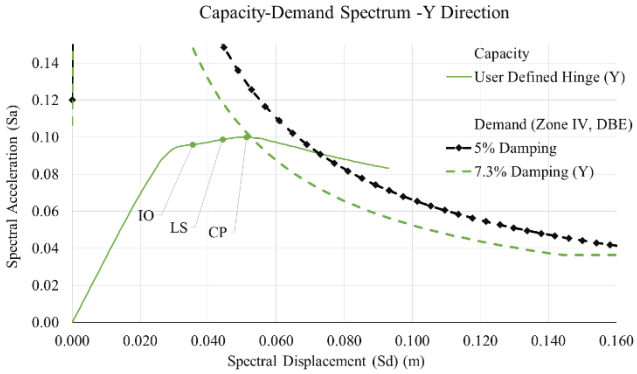

Fig. 20 Capacity-Demand Spectrum with Damping (Y – Direction)

From the curves of Capacity-Demand Spectrum with reduced damping accounting element Energy dissipation of the structure, it is observed that the structure is in the Collapse Prevention (CP) performance Level and in Y-direction it is observed that the Structure is very close to the Life Safety (LS) Performance Level but it is currently in the Collapse Prevention (CP) Performance Level only. From the evaluation of building, it is observed that the building needs to be retrofitted to provide additional damping for qualifying the performance level beyond IO Level. The building will be retrofitted using friction Damper and Steel Bracings. The methodology of analysis and design of Friction damper and Steel Bracings is discussed in further section.

RETROFITTING OF RC BUILDING

The retrofitting of structures is the process of increasing the capacity of the existing structures. Previous studies have shown improved response by using the hybrid retrofitting method, which includes Friction damper and Steel Bracings. In this section the methodology for designing, modeling and analysis using SAP2000 (2021) is provide for Dampers and Steel Bracings. The comparisons of the response of the Structure with and without retrofitting is carried out.

1. Retrofitting using Friction Damper

The hysteretic loop of the friction dampers is perfectly rectangular, similar to perfectly elasto-plastic material, the friction dampers can be modeled as fictitious plasticity element having an axial yield force equal to slip load and a member stiffness equal to brace stiffness (Jia, 2017) Moreover, in X-braced frames with friction dampers, when tension in one brace causes the damper to slip, it shortens the other brace, preventing buckling. In the next half cycle, this brace prepares to force the damper to slip in tension. The analysis requires each brace to be modeled for tension and compression slip at nearly zero load without buckling. To simplify FE analysis, the nonlinear link element is modeled with the same yielding force for tension and compression, despite the preference in FE analysis for a single yielding value, regardless of the axial force sign.

Following are the parameters required for modelling of friction damper in SAP2000 (2021) as per the damper manufacturer Pall dynamics, and Quaketek. The friction damper is added as the link element in

SAP2000 (2021). The link type is selected as Plastic (Wen). The Wen Model Parameters required to model the friction damper are as follows.

General Properties of the Link properties	Non-Linear Properties of the Link properties
Link type = Plastic (Wen)	Effective stiffness = Brace stiffness =*Ke=AE/L* (Tension-compression brace)
Mass (M) = Mass of the Damper (M1) + Mass of the Brace (M2)	Effective Damping = 0
Weight = M x g	Post Yield Stiffness Ratio = 0.0001
Rotational Inertia R1 = R2 = R3 = 0	Yielding Exponent = 10
Deformation DOF (Direction) U1 = (axial)	

where, A=Area of Brace, E = Modulus of Elasticity of Brace, L=length of Damper

The yielding strength ratio and Yielding exponent is consider based on the work of Couch et al. (2023); Sadeghi et al. (2021); Pilorgé (2018).

Once the slip load is obtain, the bracings for the damper can be finalized based on the Tension-Compression member design. The slip load is calculated based on the optimum slip load design method for friction damper from the study carried by Armaly et al. (2019). The study suggested that, the range of slip load can be estimated from the static analysis of the structure given the horizontal story shear forces, so the slip load in specific story can be estimated by:

$$\text{Slip Load} = \frac{1}{3}\left[\frac{\text{Story Shear}}{\text{Number of Dampers in the Storey}}\right] \tag{23}$$

Total 40 Nos. of Friction damper were assigned in X and Y direction each, in which 8 Nos. of damper were assigned per floor in the group of 2 dampers each at 4 locations in XZ and YZ plane of Building as shown in Figure 21. The Storey shear force calculation is shown in Table 3. Here, the base shear from analysis is obtained as 1640.80 kN and 1719.539 kN in X and Y direction of the Structure respectively. The Calculation of Strain energy and Optimum slip Load is shown in Table 4.

Table 3: Storey Shear Calculation

Story	Height (H) (m)	Dead load (kN)	LL @ 25% (kN)	Total floor load (W)	$W*H^2$	Distribution along Height	Lateral force (kN)		Story Shear (kN)	
							X-dir.	Y-dir.	X-dir.	Y-dir.
4th Floor	15	1523.4	225	1748.40	393390.00	0.393	675.96	645.00	675.96	645.00
3rd Floor	12	2024.4	225	2249.40	323913.60	0.324	556.58	531.09	1232.53	1176.09
2nd Floor	9	2024.4	225	2249.40	182201.40	0.182	313.07	298.74	1545.61	1474.83
1st Floor	6	2024.4	225	2249.40	80978.40	0.081	139.14	132.77	1684.75	1607.60
Ground Floor	3	2024.4	225	2249.40	20244.60	0.020	34.79	33.19	1719.54	1640.80
		9621.00	**1125**	**10746.00**	**1000728.00**		**1719.54**	**1640.80**		

Table 4: Strain Energy and Slip load Calculation

Story	Height (H) (m)	Story Shear (kN)		Story displacement in (m)		Strain energy (kN-m)		Optimum slip load (kN) per damper	
		X-dir.	Y-dir.	X-dir.	Y-dir.	X-dir.	Y-dir.	X-dir.	Y-dir.
4th Floor	15	675.96	645.00	0.105	0.107	35.479	34.500	28.16	26.88
3rd Floor	12	1232.53	1176.09	0.094	0.094	57.892	55.270	51.36	49.00
2nd Floor	9	1545.61	1474.83	0.074	0.073	57.219	53.509	64.40	61.45
1st Floor	6	1684.75	1607.60	0.049	0.047	41.383	38.044	70.20	66.98
Ground Floor	3	1719.54	1640.80	0.022	0.021	19.167	17.595	71.65	68.37
					$\sum$	**211.141**	**198.918**		

Further, for the each optimum slip loads the box section is considered for damper and is designed for Tension and Compression member as per (IS 800, 2007). The ISB 72X72X4.8 is considered for brace stiffness from IS 4923 (1997). The parameters of the Friction dampers for modeling is shown in Table 5 and Table 6. The value of E = 2 x 10^5 MPa is taken for steel.

Table 5: Damper Parameters (X-direction)

Sr. No.	Location	Section area (mm^2)	Diagonal length (m)	Mass (kg)	Weight (kN)	Effective stiffness (kN/m)	Slip load (Yield strength) (kN)	Post Yield stiffness ratio	Yielding exponent
1	4^{th} Floor	1231	5	48.3	473.82	49240	28.16	0.0001	10
2	3^{rd} Floor	1231	5	48.3	473.82	49240	51.36	0.0001	10
3	2^{nd} Floor	1231	5	48.3	473.82	49240	64.40	0.0001	10
4	1^{st} Floor	1231	5	48.3	473.82	49240	70.20	0.0001	10
5	Ground Floor	1231	5	48.3	473.82	49240	71.65	0.0001	10

Table 6: Damper Parameters (Y-direction)

Sr. No.	Location	Section area (mm^2)	Diagonal length (m)	Mass (kg)	Weight (kN)	Effective stiffness (kN/m)	Slip load (Yield strength) (kN)	Post Yield stiffness ratio	Yielding exponent
1	4^{th} Floor	1231	5.83	56.32	552.48	42229.846	26.88	0.0001	10
2	3^{rd} Floor	1231	5.83	56.32	552.48	42229.846	49.00	0.0001	10
3	2^{nd} Floor	1231	5.83	56.32	552.48	42229.846	61.45	0.0001	10
4	1^{st} Floor	1231	5.83	56.32	552.48	42229.846	66.98	0.0001	10
5	Ground Floor	1231	5.83	56.32	552.48	42229.846	68.37	0.0001	10

The dampers are then assigned to model as shown in Figure 21. Time History (TH) analysis is performed using El Centro earthquake data. The TH of El Centro earthquake record is modified to have compatibility with IS:1893 (2016) response spectrum of Zone IV, Soil Type II.

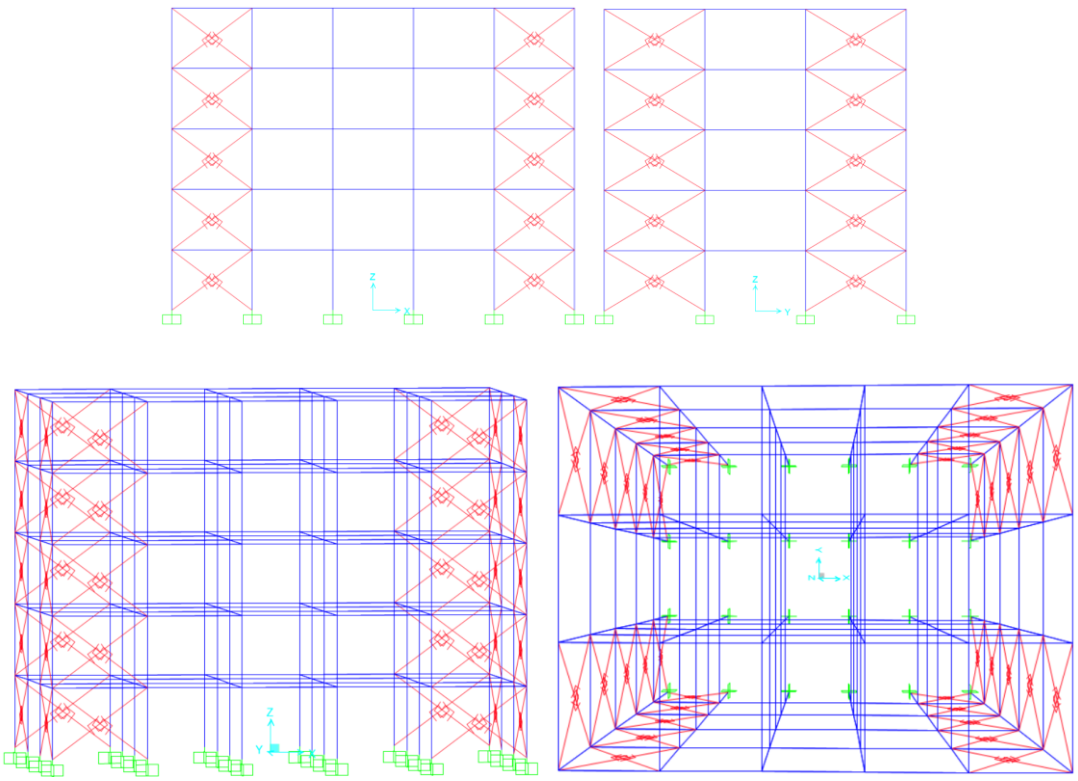

Fig. 21 Friction Damper (a) X direction (b) Y direction (c) 3D view

The compatible TH record is shown in Figure 22. The Comparison of Inter-Storey drifts results is carried out and shown in Figure 23.

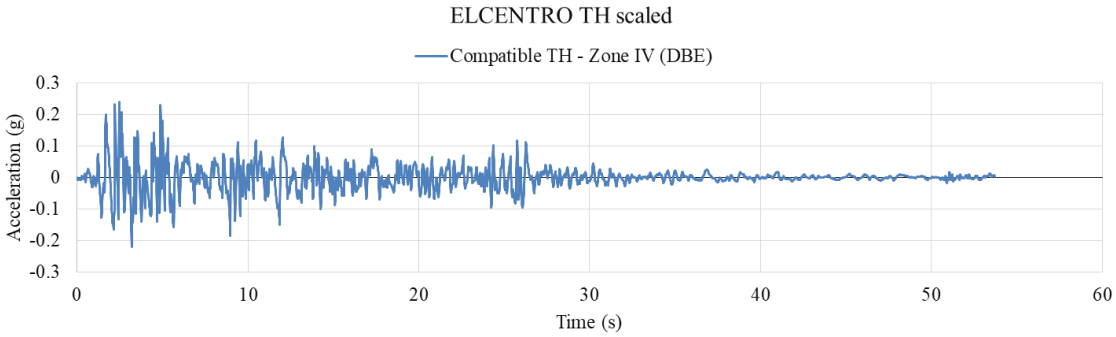

Fig. 22 Modified El Centro TH compatible to IS:1893 (2016), Z-IV

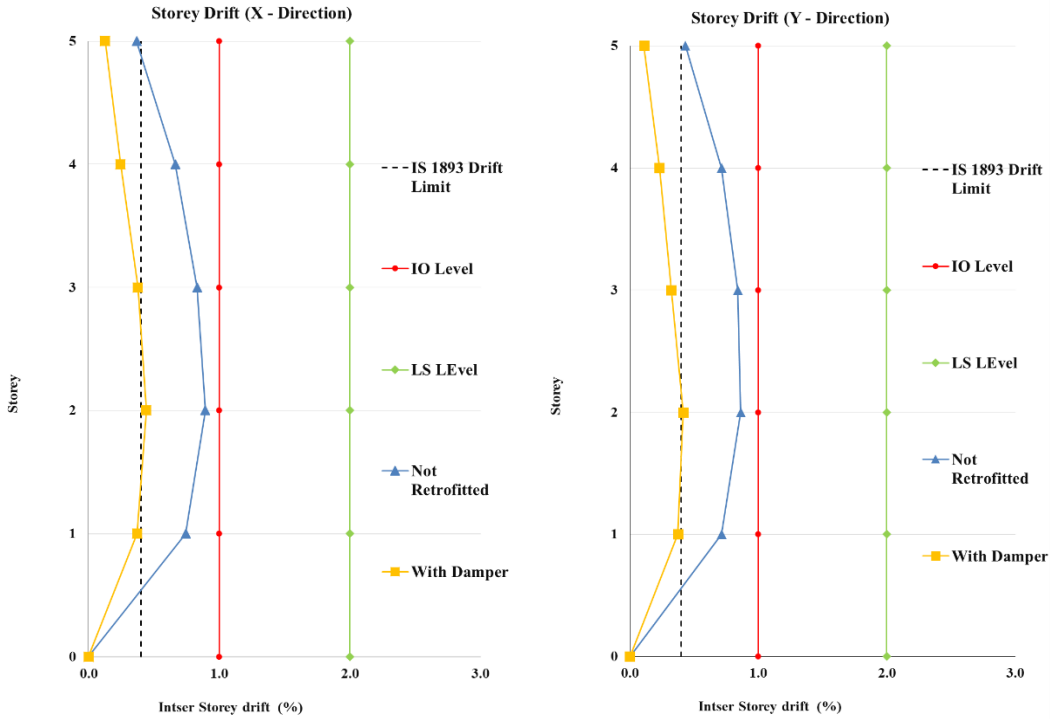

Fig. 23 Comparison of Inter Storey Drift results (a) X-Direction (b) Y-Direction

The drift results shows that the Peak inter-Storey drift is reduce by 50.56 % in X-direction and 51.16% in Y-direction. Further the Performance of the structure is checked by accounting the energy dissipation from Dampers. From the Time history analysis, the Hysteresis loop of a friction damper at Ground Floor in X-direction is shown in Figure 24. From the figure it is observed that the damper is slipped, which was designed for the slip load of 71.65 kN.

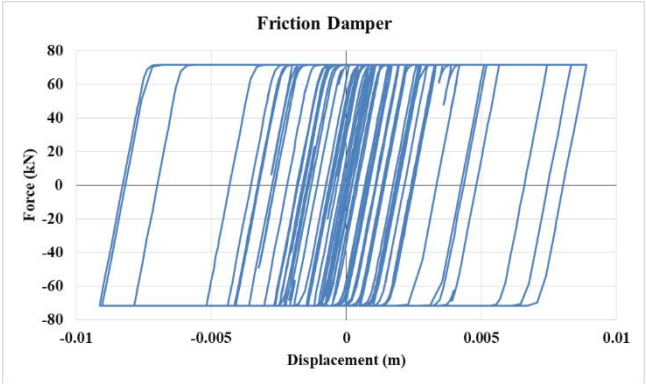

Fig. 24 Hysteresis loop of Friction Damper

The energy dissipation from the all Friction dampers is carried out, the Area under the hysteresis loop of friction damper is calculated and total Energy Dissipation (E_D) is obtained as shown in Table 7. The demand spectrum is generated from compatible El Centro TH data and it is reduced to the effective damping of obtained accounting the Energy dissipation of Dampers. The Capacity-Demand spectrum of structure retrofitted with Damper is shown in Figure 25 and Figure 26.

Table 7: Energy Dissipation Calculation for Friction Dampers

Description	X direction	Y direction
Total Energy Dissipation ***(E_D)*** (kN-m) =	84.105	86.747
Strain Energy ***(Eso)*** (kN-m) =	211.141	198.918
Hysteresis damping from Friction Damper ***(β_o)*** =	0.032	0.035
Inherent damping ***($\beta_{elastic}$)*** =	0.050	0.050
Effective Damping (β_{eff})=	0.082	0.085

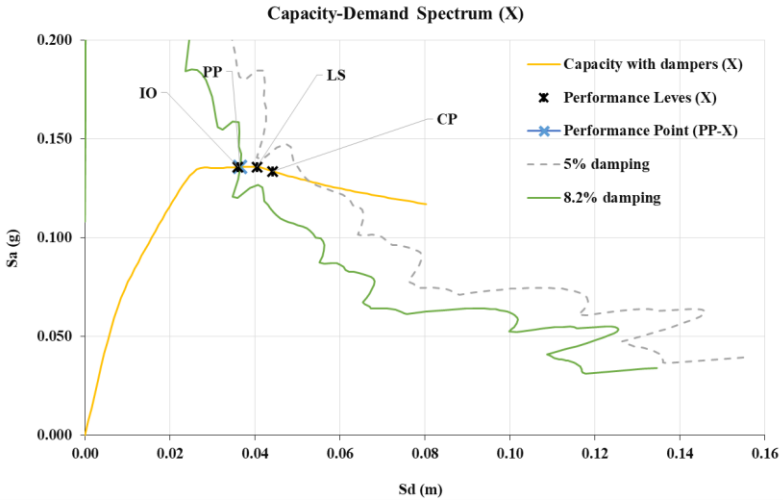

Fig. 25 Capacity Demand Spectrum (X-Direction)

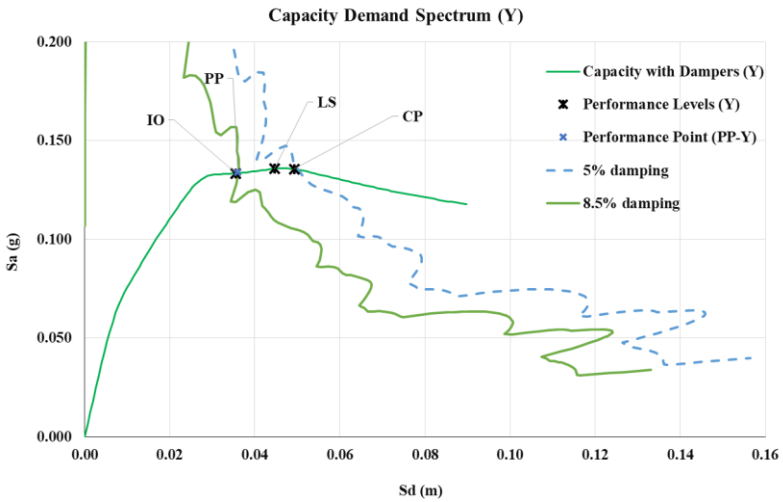

Fig. 26 Capacity Demand Spectrum (Y-Direction)

The Capacity Demand-Spectrum of the structure shows that the Structure is still in LS performance level. It is observed that Damper alone is not sufficient to qualify the structure for Immediate Occupancy (IO) performance level. Further it is required to retrofitting of the structure and for that Steel Bracings are used.

2. Retrofitting using Steel Bracing

The retrofitting of structure using steel bracings alone was carried out. Analysis results showed that the retrofitted structure shows higher capacity and the performance of the structure is also improved. So the retrofitting by using Steel bracing has shown the improved performance level of the structure. But, after retrofitting the structure with bracings higher forces is observed in the column as shown below in Table 8, also the natural frequency of structure is increased by 39.87% and 35.45% in Y and X direction respectively. To avoid such difference in the dynamic characteristics of structure, the hybrid retrofitting method combining the Friction damper and steel bracings (Hybrid retrofitting) both are used.

Table 8: Comparison of Forces in Column

Sr. No.	Description	Original Structure	Retrofitted with Bracings	% difference w. r. to Original Structure
1	Column No.5 (located at top Corner)			
	Axial Force (kN) (X-Direction)	29.80	26.69	10.42
	Axial Force (kN) (Y-Direction)	25.81	41.80	(61.95)
	Shear Force (kN) (X-direction)	39.10	48.11	(23.05)
	Shear Force (kN) (Y-direction)	44.21	58.93	(33.29)
	Bending Moment (kN-m) (X-direction)	65.44	80.42	(22.89)
	Bending Moment (kN-m) (Y-direction)	74.87	100.18	(33.81)
2	Column No.41 (located at bottom in (x-z) plane)			
	Axial Force (kN) (X-Direction)	681.76	1871.33	(174.49)
	Shear Force (kN) (X-direction)	53.96	52.99	1.79
	Bending Moment (kN-m) (X-direction)	81.24	79.83	1.74
3	Column No.11 (located at bottom in (y-z) plane)			
	Axial Force (kN) (Y-Direction)	763.07	1641.88	(115.17)
	Shear Force (kN) (Y-direction)	53.98	52.97	1.88
	Bending Moment (kN-m) (Y-direction)	81.17	79.85	1.62

3. Hybrid Retrofitting using Friction Damper and Steel Bracings

The design of steel bracings is carried out based on the Storey shear force requirement that is exceeding the capacity of column or column shear strength. The calculation of column shear strength (V_c) is carried out based on the IS:465 (2000), clause 40.2.2. The calculation of the column shear strength is shown in Table (9). Here, δ is the factor obtained from IS:465 (2000) and *Pu* is the axial load on column from the analysis.

Table 9: Calculation of column shear strength

δ	Pu (kN)	Column No (from SAP Model)	V_c (kN)
1.39	464.99	1	67.43
1.50	723.002	6	72.90
1.50	723.002	11	72.90
1.39	464.99	16	67.43
1.50	663.541	21	72.90
1.50	901.135	26	72.90
1.50	901.135	31	72.90
1.50	663.541	36	72.90
1.50	673.375	41	72.90
1.50	919.322	46	72.90
1.50	919.322	51	72.90
1.50	673.375	56	72.90

δ	Pu (kN)	Column No (from SAP Model)	V_c (kN)
1.50	673.375	61	72.90
1.50	919.322	66	72.90
1.50	919.322	71	72.90
1.50	673.375	76	72.90
1.50	663.541	81	72.90
1.50	901.135	86	72.90
1.50	901.135	91	72.90
1.50	663.541	96	72.90
1.39	464.99	101	67.43
1.50	723.002	106	72.90
1.50	723.002	111	72.90
1.39	464.99	116	67.43
		∑ =	**1,727.73**

The total Storey shear force obtained from the pushover analysis is found out as 2185.40 kN and 2085.32 kN in X and Y direction of the structure respectively. The calculation of the required axial force in tension and compression for the Bracings is shown in Table 10 for X and Y direction.

Table 10: Calculation of Bracing force

	X direction		Y direction	
Total Shear =	2185.40	kN	2126.27	kN
Total shear Capacity of Columns =	1727.73	kN	1727.73	kN
force required for Bracings =	500.58	kN	398.54	kN
for each grid in the direction =	250.29	kN	199.27	kN
Nos. of Bracings per grid =	2.00	Nos	2.00	Nos
horizontal force =	125.14	kN	99.64	kN
Axial force =	100.12	kN	85.44	kN

After obtaining the axial force requirement for bracings, the Square Hollow Sections is selected from IS:4923 (1997). The selected section is ISB 72X72X4.8 and the design checks for the axial load is carried based on the IS:800 (2007) for tension and Compression member which includes Gross Section Yielding, Net section rupture Yielding, Block Shear and Buckling check. The Designed Bracing sections are also satisfying the requirements specified in IS:15988 (2013). The bracings were assigned to the model of the structure as shown in Figure 27. After assigning the Bracings to the structure analysis is performed.

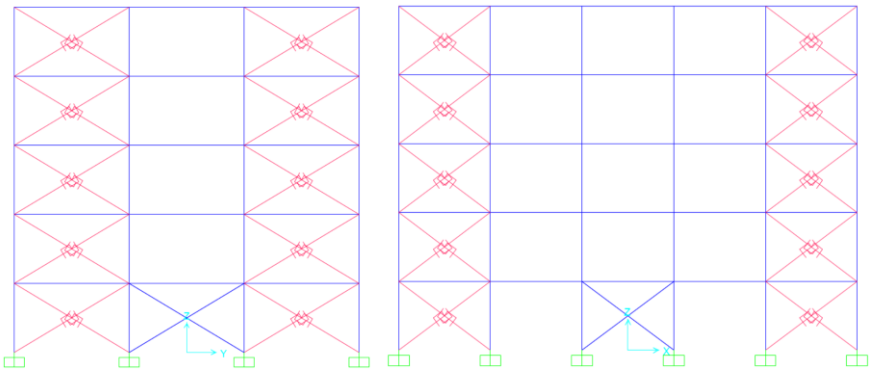

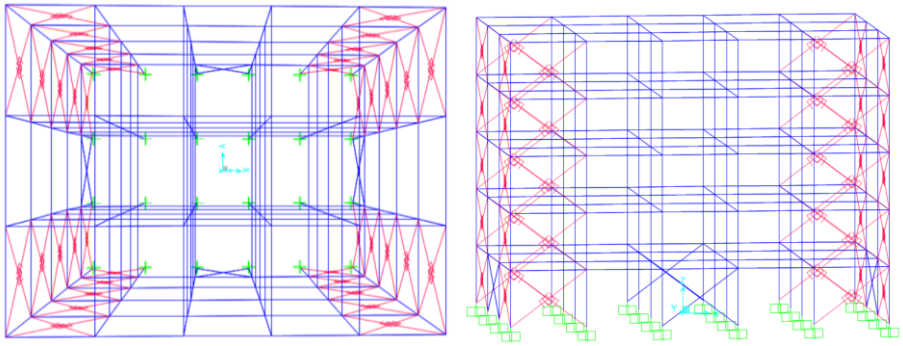

Fig. 27 Hybrid retrofitting (a) YZ plane (b) XZ plane (c) Top view (d) 3D view

The pushover analysis is performed to obtain the capacity of the structure and Time history analysis is performed to get the Energy dissipation from the dampers. Here the Element Energy dissipation of damper is calculated and the effective damping of 8.1% and 8.4% is for X and Y direction respectively. Further this damping was used to generate reduced demand spectrum of compatible El Centro Time history. The Capacity-Demand spectrum of structure is shown in the Figure 28 and Figure 29.

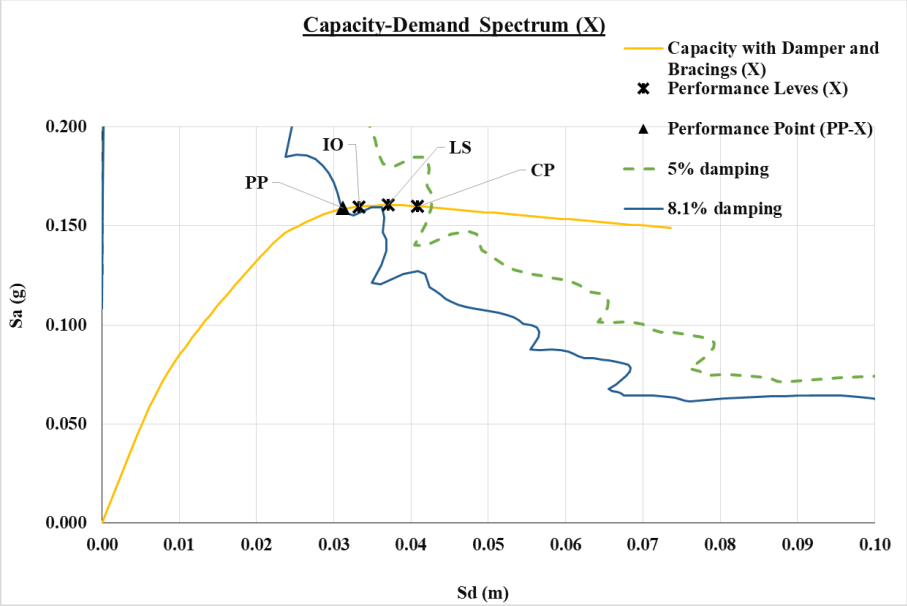

Fig. 28 Capacity-Demand spectrum with Hybrid retrofitting in X-direction

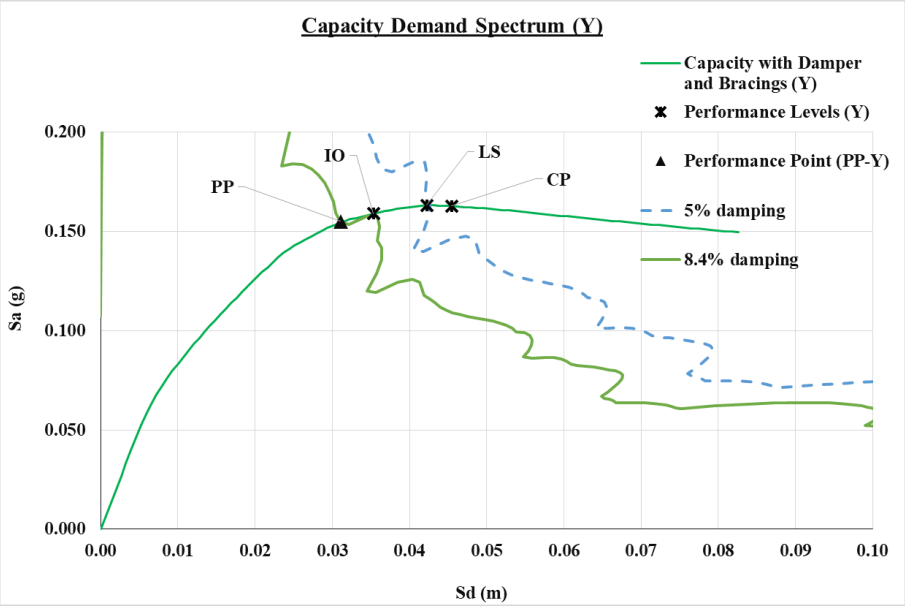

Fig. 29 Capacity-Demand spectrum with Hybrid retrofitting in Y-direction

The structure is qualified for IO performance level. All the element Hinges are found within IO level. The Storey drifts of 0.46% and 0.50% is observed, which is acceptable for IO performance level as per FFMA 356 (2000). The drift results are compared in the Figure 30.

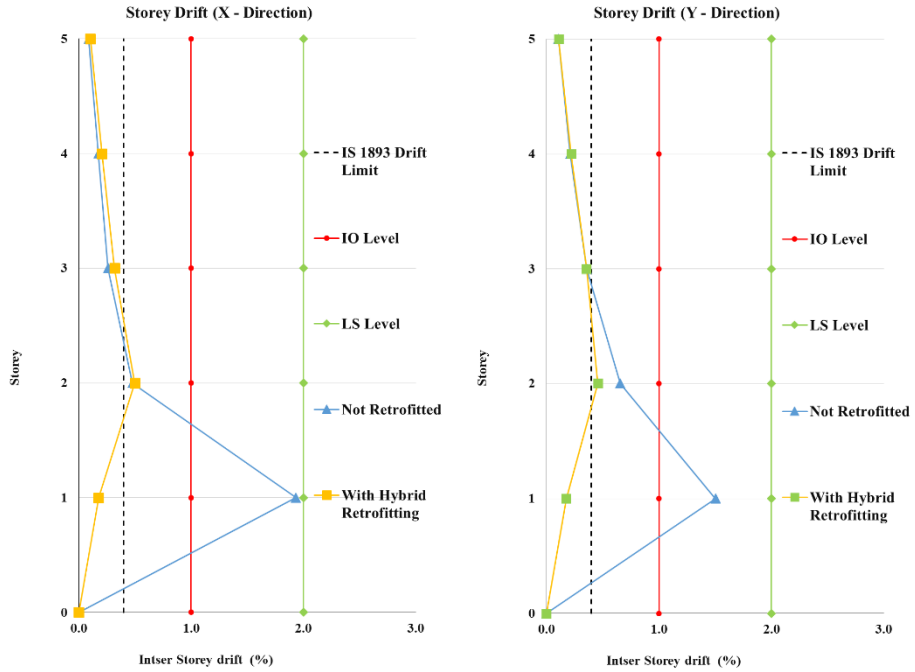

Fig. 30 Storey drifts Comparison at performance level after Hybrid retrofitting

The fundamental period of vibration of structure is found out as 0.985 Sec. and 0.947 Sec. in Y and X direction respectively, which indicates the reduction of 7.84% and 7.76% in 1st and 2nd mode of vibration respectively. Hence this methodology has improved the performance of the structure without significant impact on the time period of the structure.

CONCLUSION AND DISCUSSION

In the present work, an Existing G+4 RC building, designed for Gravity loads only based on IS:456 (2000) is considered for performance evaluation. The Pushover analysis is carried out to obtain the capacity of structure. Detailed methodology of modeling, material characteristics, and Moment-rotation

characteristics, procedures for performing the pushover analysis based on the User defined hinge characteristics of beam and Column elements is discussed. The validation of the methodology is done with the experimental test of Beam-column joint. The capacity based on the user defined hinge results is showing good match with the experimental work, while default hinge is showing higher capacity of joint. It is suggested to use the validated user-defined hinges. To evaluate the realistic capacity of the existing RC structure the required hinge characteristics can be obtained from the actual material properties of the structure by collecting the samples using the NDT testing, and after testing the materials, the material models should be calibrated, verified and used for the generating the Moment Rotation characteristics.

Further the user defined hinge characteristic cases are considered for performance evaluation. The performance criteria based on the Element Moment –rotations acceptance criteria from ASCE 41 (2013) is considered. For demands the IS:1893 (2016) based response spectrum is considered. Further it is observed that the capacity of structure is not intersecting with Zone V demand spectrum but it is intersected with the Zone IV demands. The Zone IV, soil type II demand spectrum is considered to qualify the structure. The Pushover analysis results at intersection (without retrofitting) of the Capacity-Demand Spectrum shows that,

i. The structure is found in Collapse Prevention (CP) performance level.
ii. The inter-Storey drift of 1.93% in X-direction and 1.5 % in Y-direction is observed.

Further the Element energy dissipation of the Beam and Column is considered for the hinges yielded during the pushover analysis. Accounting the Total Energy dissipation of structure, the reduced demand spectrum of 7.7% and 7.3% is obtained for X and Y direction respectively and with these demands the structure is found in Collapse Prevention performance level. While, the ATC 40 (1996) Capacity Spectrum method in SAP2000 (2021) to obtained damping of whole structure provided the 12.1% and 11.6% of damping in X and Y direction respectively, which is observed much more as compare to the element level damping of the structure. Hence, Element level damping is more appropriate and it is recommended in evaluating the performance.

The Time history analysis of the structure is carried out after modeling the dampers and the performance of the structure is evaluated by accounting the energy dissipation from Dampers. The results shows that the dampers are providing 3.2% and 3.5% of additional damping to the structures in x and Y directions. Using dampers alone the structure is in LS performance level. Hence it is concluded that Dampers alone are not suitable in the existing structures designed based on IS:456 (2000) to achieve IO performance Level. Further, retrofitting is required to qualify and improve the performance level of structure.

The performance of the structure is evaluated by combination of Friction damper and steel bracings technique (Hybrid retrofitting). The analysis results at intersection (with Hybrid retrofitting) of the Capacity-Demand Spectrum shows that,

i. The structure is found in Immediate Occupancy (IO) performance level.
ii. The inter-Storey drift of 0.46% in X-direction and 0.5 % in Y-direction is observed.

From the analysis, it is found that the dampers were able to reduce the demand by 3.1% and 3.4% for the structure in X and Y direction. The structure is qualifying the IO Performance level. The Inter-storey drifts of the structure is also reduced and observed within 1%.

RECOMMENDATIONS AND FUTURE SCOPE

Though in the present problem, shear effects may not be significant due to smaller sizes and in general it is suggested to consider the shear effects. In the present study, effect of vertical normal loads and vertical excitation is not considered. The assumptions are reasonable as mentioned in the text. Nevertheless, it is suggested to consider these loading effects for evaluating realistic capacities and performances.

REFERENCES

1. Armaly, M., Damerji, H., Hallal, J. and Fakih, M. (2019). “Effectiveness of Friction Dampers on the Seismic Behavior of High Rise Building VS Shear Wall System”, *Engineering Reports*, Vol. 1, pp. 12075. https://doi.org/10.1002/eng2.12075.
2. ASCE 41 (2013). “Seismic Evaluation and Retrofit of Existing Buildings”, *American Society of Civil Engineers*, Virginia, USA. https://doi.org/10.1061/9780784412855.

3. ATC 40 (1996). "Seismic Evaluation and Retrofit of Concrete Buildings", *Applied Technology Council*, California, USA.
4. Badoux, M. and Jirsa, J.O. (1990). "Steel Bracing of RC Frames for Seismic Retrofitting", *Journal of Structural Engineering*, Vol. 116, No. 1. https://doi.org/10.1061/(ASCE)0733-9445(1990)116:1(55).
5. Chaudhury, D. and Singh. Y. (2014). "Performance-Based Design of RC Frame Buildings with Metallic and Friction Dampers", *J. Inst. Eng. India Ser. A*, Vol. 95, No. 4, pp. 239-247. https://doi.org/10.1007/s40030-014-0089-4.
6. Couch, L., Tehrani, F.M., Naghshineh, A. and Frazao, R., (2023). "Shake Table Response of a Dual System with Inline Friction Damper", *Engineering Structures*, Vol. 281, pp. 115776. https://doi.org/10.1016/j.engstruct.2023.115776.
7. Dhakal, R.P. and Maekawa, K. (2002). "Path-Dependent Cyclic Stress-Strain Relationship of Reinforcing Bar Including Buckling", *Engineering Structures*, Vol. 24, No. 11, pp. 1383-1396.
8. FEMA 356 (2000). "Prestandard and Commentary for the Seismic Rehabilitation of Building", *Federal Emergency Management Agency*, Washington, DC, US.
9. Gupta, V.V., Reddy, G.R. and Pendhari, S.S. (2022). "Performance-Based Design of RC Structures Subjected to Seismic Load Using a Hybrid Retrofitting Method with Friction Damper and Steel Bracing", *Computational Engineering and Physical Modeling*, Vol. 5-1, pp. 19-35. https://doi.org/10.22115/CEPM.2022.317119.1191.
10. Gupta, V.V. (2021). "Performance-Based Design of RC Structures Subjected to Seismic Load Using a Hybrid Retrofitting Method with Friction Damper and Steel Bracing", *M. Tech. dissertation, Structural Eng. Dept.*, Veermata Jijabai Technological Institute (VJTI).
11. Golesorkhi, R., Joseph, L., Klemencic, R., Shook, D. and Vise, J. (2019). "Performance Based Seismic Design for Tall Buildings: An Output of the CTBUH Performance-Based Seismic Design Working Group", *Ed. (2), Chicago: Council on Tall Buildings and Urban Habitat (CTBUH)*. ISBN: 978-0-939493-72-2.
12. IS:456 (2000). "Plain and Reinforced Concrete - Code of Practice", *Bureau of Indian Standards*, New Delhi.
13. IS:800 (2007). "General construction in steel - Code of Practice", *Bureau of Indian Standards*, New Delhi.
14. IS:1893 (Part 1) (2016). "Criteria for Earthquake Resistant Design of Structure", *Bureau of Indian Standards*, New Delhi.
15. IS:4923 (1997). "Hollow Steel Sections for Structural Use – Specification", *Bureau of Indian Standards*, New Delhi.
16. IS:15988 (2013). "Seismic Evaluation and Strengthening of Existing Reinforced Concrete Buildings – Guidelines", *Bureau of Indian Standards*, New Delhi.
17. Jia, J., (2017). "Direct Damping Apparatus. In: Modern Earthquake Engineering", *Springer, Berlin*, Heidelberg. https://doi.org/10.1007/978-3-642-31854-2_22.
18. Kent, D.C. and Park, R. (1971). "Flexural Mechanics with Confined Concrete", *Journal of the Structural Division*, ASCE, Vol. 97, ST7, No. 2, pp. 1969-1990.
19. Mander, J.B., Priestley, M.J.N. and Park, R. (1988). "Theoretical Stress-Strain Behavior of Confined Concrete", *Journal of Structural Engineering*, Vol. 114, No. 8, pp. 1804-1826.
20. Moon, K.H., Han, S.W. and Lee, C.S. (2017). "Seismic Retrofit Design Method Using Friction Damping Systems for Old Low- and Mid-Rise Regular Reinforced Concrete Buildings", *Engineering Structures*, Vol. 146, pp. 105-117. https://doi.org/10.1016/j.engstruct.2017.05.031.
21. NICEE (2023), *National Information Centre of Earthquake Engineering*". https://www.nicee.org/Bhuj.php last accessed 2023/06/06.
22. Pall, A.S. and Marsh, C. (1982). "Response of Friction Damped Braced Frames", J. *Struct. Eng. ASCE*, Vol. 108, No. 6, pp. 1313-1323.
23. Pall, A.S. and Pall, R.T. (2004). "Performance-Based Design Using Pall Friction Dampers-an Economical Design Solution", *13th World Conference on Earthquake Engineering*, Vancouver, B.C., Canada, pp. 1955.

24. Patel, B. and Shah, D. (2010). "Formulation of Response Reduction Factor for RCC Framed Staging of Elevated Water Tank using Static Pushover Analysis", *Proceedings of the World Congress on Engineering*, Vol. 3, London, U.K, ISSN: 2078-0966.
25. Pilorgé, A. (2018). "Impact of Friction Dampers and Ductility Factor on the Seismic Response of Concrete Moment Resisting Frame Buildings", *Master of Applied Science (Civil Engineering), Thesis*, Concordia University, Canada.
26. Sadeghi, A., Abdollahzadeh, G., Rajabnejad, H. and Naseri, S.A., (2021). "Numerical Analysis Method for Evaluating Response Modification Factor for Steel Structures Equipped with Friction Dampers", *Asian Journal of Civil Eng*., Vol. 22, pp. 313-330. https://doi.org/10.1007/s42107-020-00315-2
27. SAP2000 (2021). "SAP2000 Ultimate V-21, Education and Research License (2021)", *SAP2000 Integrated Software for Structural Analysis and Design) Computers and Structures Inc.*, Berkeley, California.
28. Sharma, A., Reddy, G.R., Vaze, K.K., Ghosh, A.K. and Kushwaha, H.S. (2009). "Experimental Investigations and Evaluation of Strength and Deflections of Reinforced Concrete Beam-Column Joints Using Nonlinear Static Analysis", *BARC/2009/E/012, BARC*, Mumbai.
29. USGS (2023). *United States Geological Survey* homepage https://www.usgs.gov/programs/earthquake-hazards/earthquakes, last accessed 2023/06/06.
30. Zameeruddin, M. and Sangle K.K. (2021). "Performance-Based Seismic Assessment of Reinforced Concrete Moment Resisting Frame", *Journal of King Saud University – Engineering Sciences*, Vol. 33, No. 3, pp. 153-165. https://doi.org/10.1016/j.jksues.2020.04.005.